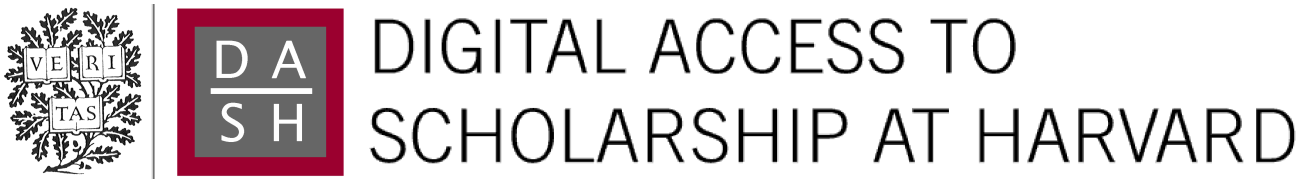

Organic-Matter Loading Determines Regime Shifts and Alternative States in an Aquatic Ecosystem

BIOLOGICAL SCIENCES: Ecology

Organic-matter loading determines regime shifts and alternative states in an aquatic ecosystem

Jennie Sirota[a], Benjamin Baiser[b], Nicholas J. Gotelli[c], and Aaron M. Ellison[b]

[a]North Dakota State University, Fargo, North Dakota 58102, USA

[b]Harvard Forest, Harvard University, Petersham, MA 01366, USA

[c]Department of Biological Sciences, University of Vermont, Burlington, VT 05405, USA

Corresponding author: Aaron M. Ellison, Harvard University, Harvard Forest, 324 N. Main St., Petersham, MA 01366, USA, Tel: +1-978-756-6178, E-mail: aellison@fas.harvard.edu

Author contributions: A.M.E. and N.J.G. designed the experiment: J.S., B.B., and A.M.E. executed the experiment: J.S., B.B., N.J.G, and A.M.E. wrote the paper.

Slow changes in underlying state variables can lead to "tipping points" – rapid transitions between alternative states ("regime shifts") in a wide range of complex systems. Tipping points and regime shifts routinely are documented retrospectively in long time series of observational data. Experimental induction of tipping points and regime shifts is rare, but could lead to new methods for detecting impending tipping points and forestalling regime shifts. Using controlled additions of detrital organic matter (dried, ground arthropod prey), we experimentally induced a shift from aerobic to anaerobic states in a miniature aquatic ecosystem – the self-contained pools that form in leaves of the carnivorous northern pitcher plant, *Sarracenia purpurea*. In un-fed controls, the concentration of dissolved oxygen ($[O_2]$) in all replicates exhibited regular diurnal cycles associated with daytime photosynthesis and nocturnal plant respiration. In low prey-addition treatments, the regular diurnal cycles of $[O_2]$ were disrupted, but a regime shift was not detected. In high prey-addition treatments, the variance of the $[O_2]$ time series increased until the system tipped from an aerobic to an anaerobic state. In these treatments, replicate $[O_2]$ time series predictably crossed a tipping point at ~45h as $[O_2]$ was decoupled from diurnal cycles of photosynthesis and respiration. Increasing organic-matter loading led to predictable changes in $[O_2]$ dynamics, with high loading consistently driving the system past a well-defined tipping point. The *Sarracenia* microecosystem functions as a tractable experimental system in which to explore the forecasting and management of tipping points and alternative regimes.

Keywords: Aerobic, alternative states, anaerobic, model system, photosynthesis, regime shift, *Sarracenia purpurea*, tipping point

\body

"Regime shifts" are rapid, often unexpected shifts in the dynamics of a system caused by slow, usually directional changes in an underlying state variable (1, 2). In common usage, regime shifts reflect a shift from a more "desirable" state of the system to a less desirable one (3, 4). Regime shifts have been observed in a wide range of financial, physical, and biological systems (4), and accurate predictions and methods to avert tipping points and ameliorate the negative effects of regime shifts or even reverse them is a central focus of contemporary research in many fields (4-7).

A classic example of an ecological regime shift of broad societal concern is the shift from a clear, oligotrophic lake to a murky, eutrophic one. The basic mechanism of eutrophication is well-understood (2, 3). Increases in limiting nutrients, especially nitrogen and phosphorous (8), boost primary production by algae and phytoplankton (9). This increase in producer biomass cannot be controlled by grazers, leading to increased shading and turbidity (10). Oxygen levels drop as microbes decompose this biomass, often leading to population declines of grazers and predators and the collapse of aquatic "green" (i.e., producer-controlled) food webs (11). A similar sequence can occur if there is an excess of allochthonous inputs of organic matter (detritus) into "brown" (i.e., donor-controlled) aquatic ecosystems (12).

A key feature of regime shifts is that feedbacks among state variables (3, 13) and relationships between state variables or "drivers" (*e.g.*, carbon, nitrogen, phosphorus, or other critical energy or nutrient sources) and measured response variables (*e.g.*, turbidity, dissolved O_2 concentration, or food-web structure) can differ dramatically before and after a state change (14). For example, in oligotrophic lakes, concentrations of nitrogen (N) and phosphorus (P) are well correlated with producer biomass, but these correlations break down in eutrophic lakes (15). In

oligotrophic lakes, excess phosphorus is absorbed by benthic sediments and its release back into the water column is slow (16). But if the concentration of P in the water is continuously elevated, it can cross a threshold – a "tipping point" – beyond which the rate of phosphorus (P) recycling between lake sediments and the water column increases rapidly (16), leading to eutrophication. However, subsequent reductions of P in the water of eutrophic lakes do not shift the lake back to an oligotrophic state because, in the eutrophic state, P recycling no longer uniquely controls the state of the system (17).

A large body of theoretical work has identified a number of statistical early-warning indicators for a tipping point, defined as the point in time when a system shifts from one regime to another (7). Less attention has been paid to systematic changes in the dynamics of systems on either side of a tipping point (8), although demonstrating that alternative states exist in a system is necessary to reliably conclude that at tipping point has been passed (14). The emphasis on tipping points is perhaps unsurprising because if a tipping point can be detected far enough in advance, then a regime shift may be averted (3–6). However, modeling studies have shown that the lead time required to avert a regime shift can be unacceptably long (5, 6), so additional attention must be paid to understanding dynamics both before and after state changes as a first step towards determining how to manage or reverse them (*e.g.*, 18, 19). The now-standard retrospective analyses of lengthy time series of observational data can identify tipping points, illustrate that an early warning was available if it had been looked for, and document alternative states (1, 3-4, 20). Prospective forecasting, however, requires a different approach.

Experimental induction of regime shifts would provide a workable platform from which researchers could generate detailed knowledge of initial and final states and the tipping point in between them. An experimental system also would facilitate the development, testing, and

analysis of early-warning indicators of tipping points, prospective interventions to delay or prevent regime shifts, and methods to shift the system between alternative states. Unfortunately, such experiments are rare (2), and mathematical modeling of tipping points and regime shifts has far outpaced available empirical data (7, 21). However, three recent microcosm studies have experimentally induced tipping points in populations of single species of microorganisms and tested whether 'critical slowing down' (*csd*) of population density indicates a rapidly approaching tipping point (22-24). These studies revealed that signals of a tipping point could be detected as early as eight generations before a transcritical threshold was crossed (22), that systemic stochasticity could reduce the signal-to-noise ratio in early-warning indicators of tipping points (23), and that fold bifurcations in system dynamics occurred as a catastrophic threshold between different system states was crossed (24). Although consistent with theoretical predictions, these studies on single species in highly simplified environments are not easily extrapolated to eutrophic aquatic ecosystems.

In this study, we experimentally induced a tipping point and a regime shift from an aerobic to an anaerobic state in an entire aquatic ecosystem: the aquatic assemblage of microbes and invertebrates found in the leaves of the northern pitcher plant, *Sarracenia purpurea* (25). This *Sarracenia* "microecosystem" is ideal for studying tipping points and regime shifts for three reasons. First, it is a naturally occurring, yet tractable and replicable experimental system in which water-filled pitchers host a well-characterized, five-trophic level, detritus-based food web (26, 27). Second, its carbon (photosynthetic) and nutrient-cycling dynamics are well characterized and understood (28–30), so mechanistic linkages can be made between organic-matter loading (*i.e.*, prey addition) and persistence of, or transitions between, aerobic and anaerobic states (See SI Appendix, a model of the *Sarracenia* system). Finally, because it

naturally exists in both aerobic and anaerobic states, the *Sarracenia* system can be viewed as a model system for understanding eutrophication in freshwater ponds and lakes, which have provided some of the best examples of tipping points and regime shifts. Most systems studied so far, including the *Sarracenia* system, can shift between regimes or eventually recover from apparently catastrophic shifts (19). Moreover, our perception of the apparent long-term stability of many systems may not reflect the underlying drivers of system change (14). For these reasons, we avoid here the use of the word *stable* in "alternative stable state", and instead focus on the statistical properties of systems that emerge from controlled and replicated experiments.

The *Sarracenia* microecosystem

Sarracenia purpurea is a widespread, long-lived, perennial, North American carnivorous plant (31). The plant has pitcher-shaped leaves that open during the growing season, fill with rainwater, and capture invertebrate prey, primarily ants (32). This resource base of captured prey supports a five-trophic level food web that includes bacteria, protozoa, the bdelloid rotifer *Habrotrocha rosa* Donner, and larvae of several obligate Diptera (25, 33, 34). The *Sarracenia* food web has been characterized as a processing chain commensalism (33), but the top predators in the system—larvae of the pitcher-plant mosquito, *Wyeomyia smithii* (Coq.), and the pitcher-plant flesh-fly, *Fletcherimyia fletcheri* (Aldrich)—are not critical for breakdown of prey and translocation of nutrients to the plant; the microbes by themselves efficiently decompose and mineralize nearly all of the captured prey biomass (29).

Depending on the photosynthetic activity of the plant, the quality and quantity of captured prey, and the structure of the food web within the pitcher, the oxygen content of the liquid in pitcher in the field can vary greatly from well-oxygenated to nearly anaerobic (See SI Appendix, a model of the *Sarracenia* system). In aerobic conditions, captured prey is rapidly

shredded by larvae of the pitcher-plant midge *Metriocnemus knabii* Coq. and subsequently processed by aerobic bacteria whose populations are regulated by higher trophic levels in the food web (35). The respired carbon dioxide from the food web is taken up by the plant, which in turn releases oxygen back into the water as it photosynthesizes (28). In contrast, anaerobic conditions occur following a rapid accumulation of excess prey (often from a single pulsed input; *e.g.* (36)) that cannot be processed with sufficient speed by the animal food web (See SI Appendix, fig. S2). The daily input of O_2 to the aquatic microecosystem from plant photosynthesis and diffusion from the atmosphere cannot compensate for the slower breakdown of prey by anaerobic microbes, and concentration of dissolved O_2 remains at persistent low levels. In other words, when prey input is excessive, the *Sarracenia* ecosystem resembles lakes, streams, estuaries, and other aquatic ecosystems that have experienced increased biological oxygen demand following eutrophication (9, 12, 26).

Results and Discussion

In un-fed controls, dissolved oxygen concentration ($[O_2]$, expressed in percent, where percent O_2 in the atmosphere = 20.95 ≡ 1.26 g/L O_2 at 25 °C at Harvard Forest, 334 m above sea level) in all replicates exhibited a regular diurnal cycle associated with daytime photosynthesis and nocturnal plant respiration (Fig. 1A; See SI Appendix, fig. S1). In all of these control time series, there also was a slight trend towards increasing $[O_2]$ over the course of each 4-day experiment (See SI Appendix, fig. S6). In the two lowest prey-addition treatments (0.125 mg ml^{-1} d^{-1} or 0.25 mg ml^{-1} d^{-1} added nutrients), diurnal cycles of $[O_2]$ became irregular and illustrated a complex pattern of fluctuations (Fig. 1B, 1C). At the two highest prey-addition treatments (0.5 mg ml^{-1} d^{-1} or 1.0 mg ml^{-1} d^{-1} added nutrients), the diurnal cycle of $[O_2]$ was restored, albeit with a greatly diminished

amplitude and at a substantially lower overall [O_2] level (Fig. 1D, 1E). The frequency distribution of day-time [O_2] was distinctly multimodal (Fig. 2), and depended on prey additions, not PAR, which was unimodal with a single day-time mode of 388 μmol m^{-2} s^{-1} (See SI Appendix, fig. S10-S12, table S2). As in many other systems, these prominent modes are most parsimoniously explained as resulting from nonlinear responses of the pitcher-plant microecosystem to variation in prey availability and its subsequent decomposition (See SI Appendix, analysis of frequency distribution of daytime oxygen concentration). In short, experimental additions of organic-matter created and sustained aerobic and anaerobic states, and initiated a transition from aerobic to anaerobic states.

A loess model effectively detrended and de-cycled the control time-series data of [O_2], yielding nearly constant residuals in these time series (Fig. 1F; See SI Appendix, fig. S13-S16). The [O_2] time series of all prey-addition treatments still exhibited some periodicity relative to the controls (Fig. 1G-1J), but quantitative analysis of structural changes—different regimes—in each time series revealed statistically-significant break points only in the two highest prey-addition treatments (0.5 mg ml^{-1} d^{-1} and 1.0 mg ml^{-1} d^{-1} added nutrients). In each of these two treatments, tipping points were detected in five of six replicates (temporal locations of individual time series indicated by the vertical cyan lines in Fig. 1I, 1J; break points of the averaged time series indicated by the vertical red lines in Fig. 1I, 1J). The break point in the two highest prey-addition treatments occurred on average 44.6 hours after the start of the feeding experiment and differed between treatments on average by only 114 minutes ($t_{[4]} = 0.8655$, $p = 0.4$, paired *t*-test), in spite of a doubling of the food addition rate. These results suggest that there is a threshold concentration of organic-matter loading at ≈0.5 mg ml^{-1} d^{-1} that can reliably induce a tipping point and regime shift in the *Sarracenia* microecosystem.

In addition to differences in time-series dynamics, the statistical moments and trends of the $[O_2]$ time series differed significantly among the four prey-addition treatments and the controls (Fig. 3; Table 1). With increasing prey-addition, there were decreases in the skewness and temporal trends of $[O_2]$ (Fig. 3) and the variance of the $[O_2]$ time series increased with increasing prey additions up until the system shifted from an aerobic to an anaerobic state (See SI Appendix, fig. S16). Within the 0.5 mg ml^{-1} d^{-1} prey-addition treatment—the lowest feeding level for which we observed a state change—the time-series mean was significantly higher ($t_{[5]}$ = 8.84, $P < 0.001$) before the regime shift than afterward, and the temporal trend in $[O_2]$ shifted from declining before the system shifted from aerobic to anaerobic to flat after the regime shift ($t_{[5]} = 3.76$, $P = 0.007$) (compare the colored box plots in Fig. 3). A statistically stronger, but qualitatively similar result was found in the 1.0 mg ml^{-1} d^{-1} prey-addition treatment: all three statistical moments were higher, and the temporal trend in $[O_2]$ was significantly more negative, before the regime shift than after it (mean: $t_{[5]} = 7.28$, $P < 0.001$; variance: $t_{[5]} = 5.46$, $P = 0.001$; skewness: $t_{[5]} = 4.93$, $P = 0.002$; slope: $t_{[5]} = 3.39$, $P = 0.01$). We note, however, that these patterns do not necessarily indicate *csd*. Deterministic dynamics could cause manipulated microecosystems to simply diverge further from the controls, leading to an increase in variance that would be unrelated to *csd*. Thus, evidence for *csd* would be better identified from analysis of individual time series or of replicate time series within each treatment (see SI Appendix, supplemental analysis of time-series data).

The relationship between $[O_2]$ and light available for photosynthesis—the primary driver of O_2 production by the plant—differed between the two states (Fig. 1K-1O; See SI Appendix, fig. S13, S14). In the un-fed controls, the trajectory in phase space was virtually identical for all 4 days of the time series (Fig. 1K), and illustrated normal diurnal cycling of photosynthesis and

respiration. As the prey-addition rate was increased, the replicated trajectories became more separated for the early and later parts of each time series (Fig. 1L, 1M). At the two highest feeding levels, the different regimes were distinctly separated (either side of the red circle in Fig. 1N, 1O). Such changes in the relationships between drivers and response on either side of a tipping point are consistent with theoretical and empirical studies of alternative states in ecological systems (14, 18, 19).

Conclusions

The results presented here illustrate that, with modest organic-matter loading, we can predictably induce a regime shift in a fully functioning, multi-trophic, detritus-based (donor-controlled) ecological system. Although there was some variability between replicate ecosystems receiving the same prey additions, the variance within treatments was relatively small, and the system responded in characteristic and repeatable ways to increases in the feeding rate (Fig. 1, 2; See SI Appendix, fig. S12, S14). These results suggest that organic-matter loading not only triggers the state change from the aerobic to the anaerobic state, but that decomposition of prey (35) and biological oxygen demand are the primary drivers that control the dynamics both before and after a tipping point (Fig. 3; See SI Appendix, fig. S3, S8-S10).

The experimental induction of alternative states in the *Sarracenia* microecosystem provides some support for theoretical predictions of increasing variance in time series prior to a regime shift. More importantly, however, this study highlights the possibilities of a tractable experimental system with which to explore tipping points, regime shifts, and alternative states. Future work with this system will involve identifying biologically based early-warning indicators of tipping points. We hypothesize that such biomarkers, including genomic and proteomic

markers derived from microbial activity (37), can provide more lead time for intervention than measurements of traditional environmental variables such as $[O_2]$, which may be easier to measure but are themselves driven by underlying biological processes.

Materials and Methods

We explored the dynamics of aerobic to anaerobic state changes in the pitcher-plant system using mathematical modeling (See SI Appendix, a model of the *Sarracenia* system) and a controlled greenhouse experiment. Replicate *Sarracenia purpurea* pitchers were inoculated with liquid collected from field plants that contained the naturally-occurring bacterial community. We then varied the prey fed to each pitcher and continuously monitored the concentration of dissolved oxygen $[O_2]$. Each individual *Sarracenia* leaf functioned as an independent ecosystem in which the response of an environmental variable (dissolved $[O_2]$) was monitored as a function of an environmental driver (organic-matter addition). We report $[O_2]$ as a percent. The percent O_2 in the atmosphere = 20.95. The greenhouse at Harvard Forest in which we did the experiment is at 334 m above sea level, where the atmospheric pressure is 0.964 that of sea level. Thus, the atmospheric density of O_2 in the greenhouse at 25 °C (within 0.5 ° of the average air and pitcher-fluid temperatures during the experiment – see below) = 1.26 g/L.

Experimental Treatments Pitcher plants were purchased from Meadowview Biological Station (Woodward, Virginia, USA) in 2010, and maintained in the Harvard Forest greenhouse for two years before the experiments were initiated in June 2012. For each of six experimental trials, we randomly selected five plants and used the most recent fully-formed pitcher (leaf) on each plant as the focal pitcher for a randomly-assigned treatment. We filled the focal pitcher on each plant with pitcher fluid collected on the first day of each trial from pitchers

249 growing in a naturally occurring *S. purpurea* population at Tom Swamp Bog in Petersham, MA
250 (42°30' N, 72°11' W), 6 km from the greenhouse. To remove macrobes and debris larger than 30
251 μm in diameter, pitcher fluid was filtered first through sterile Whatman filter paper (Whatman
252 International Ltd, Maidstone, England), and then through sterile BioRadpolyprep
253 chromatography columns (Bio-Rad Laboratories, Richmond, CA). Focal pitchers were filled to
254 slightly below their rim with homogenized filtrate. Focal pitchers varied in volume from four to
255 18 ml, and the volume of pitcher fluid dispensed into each leaf was recorded. Non-focal pitchers
256 on each plant were filled with deionized water.

257 At noon each day for four consecutive days, treated plants were fed an aliquot (0.125,
258 0.25, 0.5, or 1.0 mg ml^{-1} d^{-1}) of dried, finely-ground vespid wasp (*Dolichovespula maculata*
259 (Fabr.)) tissue that has a % C = 51.5, a C:N ratio of 5.99 : 1 and N:P:K ratios (10.7 : 1.75 : 1.01)
260 nearly identical to those of ant species (C:N = 5.9; N:P:K = 12.1 : 1.52 : 0.93) that are the most
261 common prey item of pitcher plants (30). Dissolved oxygen concentration in the pitcher fluid
262 was measured at 1-s intervals with D-166MT-1S microelectrodes (Lazar Research Laboratories,
263 Los Angeles, CA); 1-minute averages were recorded with a CR-1000 data logger (Campbell
264 Scientific, Logan, Utah). Each day when the plants were fed, oxygen electrodes were
265 recalibrated following the manufacturer's instructions. Temperature in the pitcher fluid and the
266 surrounding air were measured simultaneously with thermistors (mean air temperature = 25.45
267 °C; mean water temperature = 25.18 °C), and photosynthetically active radiation (PAR: μmol m^{-2}
268 s^{-1}) was measured 5 cm below the tops of the plants with an LI-190SA PAR sensor (Li-COR,
269 Lincoln, NE).

270 We ran six of these 4-day experimental trials. Each run consisted of five plants assigned
271 randomly to one of five different prey-addition levels (0 [unfed controls], 0.125, 0.25, 0.5, 1.0

mg ml^{-1} d^{-1}) and represented a temporal block to control for unmonitored changes in the greenhouse environment through the course of the summer. Plants were assigned randomly to treatments, interspersed randomly in trays on greenhouse tables, and treated identically in all respects other than the prey-addition level they received. Total sample size over the six replicate temporal blocks was 30 plants. There was no significant block (trial) effect on any of the test statistics (Table 1).

Data Analysis For each of the 30 plants, we generated a time series of 1-minute averages of $[O_2]$ and PAR; lengths of the time series ranged 5734-5862 observations. To facilitate averaging across replicates, we truncated the terminal observations in each series to match the shortest time series (5734 min). During daily feeding and recalibration, the $[O_2]$ series was interrupted; we used linear interpolation to fill in these missing values, which constituted < 2% of each time series.

Statistical detection and analysis of tipping points and alternative states normally is done on detrended and de-cycled time series of standardized data (7). We centered and scaled individual measurements x_i (i = 1 to t; t = 5734) of $[O_2]$ in each time series as: $z_i = \frac{x_i - \bar{X}}{\sigma_X}$. In time-series analyses, data are typically detrended and de-cycled by fitting smoother functions to a series and then calculating residuals from the fitted trend line (38). In this study, however, the control time series represents the explicit null hypothesis against which state changes due to organic-matter additions are properly measured. Thus, rather than detrending each time series in isolation, for comparative purposes we detrended the time series of data from the prey-addition treatments relative to the time-series data from the control plant within each block. Detrending against the controls is important because, in the absence of organic-matter loading, the $[O_2]$ series for the *Sarracenia* micro-ecosystem exhibits diurnal periodicity (Figure 1A), reflecting the

295 daily cycle of plant photosynthesis and respiration (28). Such periodicity can obscure early-
296 warning indicators of tipping points (39). We fit a smoothed local regression model to each of
297 the standardized control series, using the loess function in the stats library of R (version
298 2.13.1).We then de-cycled and detrended data from the enriched series by subtracting the
299 predicted (loess) values of the standardized control time series from the observed, standardized
300 values of each time series of fed pitchers. Alternative analyses of the raw time series and of time
301 series that were detrended and de-cycled individually (as opposed to relative to the controls) are
302 presented in SI Appendix (See SI Appendix, supplemental analysis of time-series data). These
303 supplemental analyses gave results that were qualitatively similar to those based on a detrending
304 of each food-addition time series relative to the control series.

305 We used the strucchange library in R (40) to test statistically for the presence of break
306 points in each of the time series (including the controls). strucchange should be applied to
307 detrended, de-cycled series; a time series without breaks is flat (slope = 1) and has mean
308 (intercept) = 0. strucchange then applies a moving window across a time series to identify the
309 optimal number of break points (change in intercept) on the basis of the residual sum of squares
310 and Bayesian information criterion; the latter imposes a penalty for the identification of multiple
311 breakpoints, and the optimal number of breakpoints may = 0. We used a conservative 2-standard
312 deviation criterion to distinguish statistically significant break points (14). Break points were
313 identified for time series only in the two highest prey-addition treatments, and for these we used
314 a simple *t*-test to compare the average time to the breakpoint.

315 Following the approach of Dakos et al. (7), we examined metric-based indicators of
316 tipping points in each time series. For the $[O_2]$ residuals of each time series, we estimated the
317 statistical moments (mean, variance, skewness) and the least-square regression slope of the

residuals versus time (a simple index of a linear temporal trend). Models of tipping points suggest that there should be an increase in the variance (See SI Appendix, fig. S16), or skewness as a breakpoint is approached (7); evidence for critical slowing down (*csd*) is best assessed by analyzing individual time series and replicate time series within each treatment (See SI Appendix, supplemental analysis of time-series data). We first used a randomized block ANOVA to test for the effect of prey-addition level on each metric calculated for the entire time series (Table 1). Next, for the two highest prey-addition treatments that exhibited statistical breakpoints, we used a matched-pairs one-sample *t*-test to test for the effects of pre- *versus* post-breakpoint differences in each metric.

In addition to the break-point tests and comparisons of statistical metrics, we visually examined plots of $[O_2]$ as a function of PAR (as in ref. 14). These plots trace the temporal dynamics of both variables simultaneously over the 4-day time series, and illustrate the separation of the time series into distinctive alternative states in the fed treatments. Fig. 1 illustrates residuals of $[O_2]$ as a function of PAR; Fig. S14 illustrates the $[O_2]$ – PAR relationship for raw $[O_2]$ data.

Data Availability All raw data and R code for the analyses, and Mathematic code for the *Sarracenia* model are available from the Harvard Forest Data Archive (http://harvardforest.fas.harvard.edu/data-archive), dataset HF205.

ACKNOWLEDGMENTS. This research was supported by NSF grants DEB 10-03938 and 11-44056 to AME and 11-44055 to NJG. Mark Van Scoy assisted with setting up the instrumentation, and Michael Lavine discussed statistical analyses with the corresponding

author. Two anonymous reviewers and the academic editor provided thorough and helpful comments that greatly improved the final paper.

References

1. Scheffer, MJ, et al. (2009) Early-warning signals for critical transitions. *Nature* 461(7260):53–59.
2. Carpenter SR, et al. (2011) Early warnings of regime shifts: a whole ecosystem experiment. *Science* 332(6033):1079–1082.
3. Carpenter SR, Brock WA (2006). Rising variance: a leading indicator of ecological transition. *Ecol Lett* 9(3):308–315.
4. Scheffer MJ, et al. (2009) Critical transitions in nature and society. Princeton Univ. Press, Princeton, NJ.
5. Contamin R, Ellison AM (2009). Indicators of regime shifts in ecological systems: what do we need to know and when do we need to know it? *Ecol App* 19(3):799–816.
6. Biggs R, Carpenter SR, Brock WA (2009). Turning back from the brink: detecting an impending regime shift in time to avert it. *Proc Nat Acad Sci USA* 106(3):826–831.
7. Dakos, V, et al. (2012) Methods for detecting early warnings of critical transitions in time series illustrated using simulated ecological data. *PLoS ONE* 7(7): e41010.
8. Carpenter SR, et al. (1998) Nonpoint pollution of surface waters with phosphorus and nitrogen. *Ecol App* 8(3):559-568.
9. Smith VH, Tilman GD, Nekola JC (1999) Eutrophication: impacts of excess nutrient inputs on freshwater, marine, and terrestrial ecosystems. *Env Poll* 100(1-3):179-196.

10. Vadeboncoeur Y, Lodge DM, Carpenter SR (2001) Whole-lake fertilization effects on distribution of primary production between benthic and pelagic habitats. *Ecology* 82(4):1065-1077.
11. Diaz RJ (2001) Overview of hypoxia around the world. *J Env Qual* 30(2):275-281.
12. Wallace JB, Eggert SL, Meyer JL, Webster JR (1999) Effects of resource limitation on a detrital-based ecosystem. *Ecol Monogr* 69(4):409-442.
13. Lawrence D, et al. (2007) Ecological feedbacks following deforestation create the potential for a catastrophic ecosystem shift in tropical dry forest. *Proc Natl Acad Sci USA* 104(52):20696-20701.
14. Bestelmeyer BT, et al. (2011) Analysis of abrupt transitions in ecological systems. *Ecosphere* 2(12):129.
15. Scheffer M, van Nes, EH (2007) Shallow lakes theory revisited: various alternative regimes driven by climate, nutrients, depth and lake size. *Hydrobiologia* 584(1):455-466.
16. Carpenter SR, Cottingham KL (1997) Resilience and restoration of lakes. *Cons Ecol* 1(1):2.
17. Carpenter SR, Ludwig D, Brock WA (1999) Management of eutrophication for lakes subject to potentially irreversible change. *Ecol App* 9(3):751-771.
18. Schröder A, Persson L, de Roos AM (2005) Direct experimental evidence for alternative stable states: a review. *Oikos* 110(1):3-19.
19. Jones HP, Schmitz OJ (2009) Rapid recovery of damaged ecosystems. *PLoS ONE* 4(5):e5653.
20. Donangelo R, et al. (2010). Early warnings for catastrophic shifts in ecosystems: comparison between spatial and temporal indicators. *Intl J Bifurc Chaos* 20(2):315–321.
21. Boettiger C, Hastings A (2013) From patterns to predictions. *Nature* 493(7431):157-158.

22. Drake, JM, Griffen BD (2010) Early warning signals of extinction in deteriorating environments. *Nature* 467(7314):456 –459.

23. Veraart AJ, et al. (2012) Recovery rates reflect distance to a tipping point in a living system. *Nature* 481(7381): 357–359.

24. Dai L, Vorselen D, Korolev KS, Gore J (2012) Generic indicators for loss of resilience before a tipping point leading to population collapse *Science* 336(6085):1175–1177.

25. Addicott JF (1974) Predation and prey community structure: an experimental study of the effect of mosquito larvae on the protozoan communities of pitcher plants. *Ecology* 55(3):475–492.

26. Ellison AM, et al. (2003) The evolutionary ecology of carnivorous plants. *Adv Ecol Res* 33: 1-74.

27. Srivastava DS, et al. (2004) Are natural microcosms useful model systems for ecology? *Trends Ecol Evol* 19(7):379–384.

28. Bradshaw WE, Creelman RA (1984) Mutualism between the carnivorous purple pitcher plant and its inhabitants. *Am Mid Nat* 112(2):294-303.

29. Butler JL, Gotelli NJ, Ellison AM (2008) Linking the brown and green: nutrient transformation and fate in the *Sarracenia* microecosystem. *Ecology* 89(4):898–904.

30. Farnsworth EJ, Ellison AM (2008) Prey availability directly affects physiology, growth, nutrient allocation, and scaling relationships among leaf traits in ten carnivorous plant species. *J Ecol* 96(1):213–221.

31. Schnell DE. (2002) Carnivorous plants of the United States and Canada. Timber Press, Portland, OR.

406 32. Ellison AM, Gotelli NJ (2009) Energetics and the evolution of carnivorous plants – Darwin's
407 "most wonderful plants in the world." *J Exp Bot* 60(1):19–42.
408 33. Heard SB (1994) Pitcher plant midges and mosquitoes: a processing chain commensalism.
409 *Ecology* 75(6):1647–1660.
410 34. Bledzki LA, Ellison AM (2003) Diversity of rotifers from northeastern USA bogs with new
411 species records for North America and New England. *Hydrobiologia* 385(1-3):193–200.
412 35. Baiser B, Ardeshiri R, Ellison AM (2011) Species richness and trophic diversity increase
413 decomposition in a co-evolved food web. *PLoS One* 6(6):e20672
414 36. Butler JL, Atwater DZ, Ellison AM (2005) Red-spotted newts: An unusual nutrient source
415 for northern pitcher plants. *Northeast Natural* 12(1):1–10.
416 37. Gotelli NJ, Ellison AM, Ballif BA (2012) Environmental proteomics, biodiversity statistics
417 and food-web structure. *Trends Ecol Evol* 27(8):436-442.
418 38. Shumway RH, Stoffer DS (2011) Time series analysis and its applications, with R examples,
419 3rd edition. Springer Science+Business Media, LLC, New York, NY.
420 39. Cimatoribus AA, Drijfhout SS, Livina V, van der Schrier G (2012) Dansgaard-Oeschger
421 events: tipping points in the climate system. *Clim Past Discuss* 8(5):4269-4294.
422 40. Zeileis A, Leisch F, Hornik K, Kleiber C (2002) strucchange: An R package for testing for
423 structural change in linear regression models. *J Stat Software* 7(2):1–38.

Figure Legends

Fig. 1. Analysis of the time series of dissolved oxygen concentration ($[O_2]$, in percent; on this scale, atmospheric $[O_2] = 20.95 \equiv 1.26$ g/L in our greenhouse) in *Sarracenia* microecosystems as a function of experimental organic-matter loading through prey addition: 0 (control), 0.125, 0.25, 0.5, or 1.0 mg ml^{-1} d^{-1} dry mass of ground wasps (n = 5734 observations of $[O_2]$ per replicate within each treatment). (**A–E**) Mean raw data $[O_2]$ time-series (blue line) and 95 % confidence intervals (grey region) for each treatment across six replicates. (**F–J**) Mean de-cycled and detrended time-series (blue line) and 95 % confidence intervals (grey region) for each treatment across six replicates. The five vertical cyan lines show the break points for the $[O_2]$ residuals of each replicate (1 of the 6 replicates did not display a significant break point); the vertical red line in each treatment shows the break point for the mean of all the series within a treatment. (**K–O**) Relationships between the primary environmental driver (photosynthetically active radiation [PAR, in μmol m^{-2} s^{-1}] and average (residual) $[O_2]$. Different color lines corresponding to the four days of each trial run. Dark blue represents day one, light blue represents day two, mustard represents day three, and brown represents day four. The red circles in plots **N** and **O** indicate the times of the switches from aerobic to anaerobic states in the two highest prey-addition treatments.

Fig. 2. Frequency distributions (number of minutes between 0900 and 1500 hours) of $[O_2]$ in the five different prey-addition treatments. The red triangles indicate the location of 4 modes in the joint distribution identified with normal mixture modeling and model-based clustering (See SI Appendix, fig. S12). The first identified mode (at 1.682 % O_2) corresponds to the mode for the distributions of the two highest prey-addition treatments (0.5 and 1.0 mg ml^{-1} d^{-1}); the second

447 (7.554 %) corresponds to the mode of the distribution of the intermediate prey-addition treatment
448 (0.25 mg ml^{-1} d^{-1}); the third (12.146%) corresponds to the mode for the lowest prey-addition
449 treatment (0.125 mg ml^{-1} d^{-1}); and the fourth (16.272 %) corresponds to the mode for the
450 distribution of the controls.
451 **Fig. 3.** Box-plots of statistical moments and least-squares regression slope coefficients of the
452 time series of [O_2]. Grey boxes represent replicates from treatments with no breakpoints (0,
453 0.125. 0.25 mg ml^{-1} d^{-1} added nutrients). Blue and brown boxes represent the values for these
454 variables in each of the two different states of the system induced by the higher levels of organic-
455 matter loading (0.5 and 1.0 mg ml^{-1} d^{-1} added prey). See Table 1 for statistical summaries of
456 treatment effects.

Supporting Online Material

Organic-matter loading determines regime shifts and alternative states in an aquatic ecosystem

Jennie Sirota[a], Benjamin Baiser[b], Nicholas J. Gotelli[c], and Aaron M. Ellison[a]

[a]North Dakota State University, Fargo, ND 58102

[b]Harvard Forest, Harvard University, Petersham, MA 01366

[c]Department of Biological Sciences, University of Vermont, Burlington, VT 05405

Contents

1. A model of the *Sarracenia* system....2
   1.1. Equations....2
   1.2. Details of the model....3
   1.3. Model behavior....7
   1.4. Programming and availability of code....10
2. Additional statistical analyses....10
   2.1. Analysis of frequency distribution of daytime oxygen concentration....10
   2.2. Supplemental analysis of time-series data....12
3. References....17

1. A model of the *Sarracenia* system

1.1 Equations

Classical (and still widely-used) models for oxygen dynamics in lakes and streams are linear and lack feedbacks (1). In contrast, the detritus-based, pitcher-plant (*Sarracenia purpurea* L.) food web (including the bacteria) occurs in a pool of water inside a living (and photosynthesizing) plant, providing an opportunity for (nonlinear) feedbacks between the food web and the plant itself (2).

Scheffer et al. (3) described a minimal model for a system that can exhibit alternative (stable) states and hysteresis between them:

$$\frac{dx}{dt} = a - bx + rf(x). \qquad \text{(Equation S1)}$$

In Equation S1, x is the ecosystem property of interest, a is an environmental factor that promotes x, b is the decay rate of x in the system, and r is the rate at which x recovers as a function f of property x. We apply this model to the pitcher-plant system, in which the ecosystem property of interest, x (concentration of dissolved oxygen [O_2] in mg ml^{-1}) is a function of interactions between the plant and its decomposing prey (w):

$$\frac{dx}{dt} = A - f(w,x) + g(x).$$

By analogy with Equation S1, A is the environmental factor that promotes oxygenation in the pitcher-plant liquid, $f(w,x)$ is the decay (loss) rate of oxygen in the pitcher-plant liquid, and $g(x)$ is a positive feedback loop by which oxygen concentration in the pitcher fluid recovers as a function of available oxygen, which increases from photosynthesis, but decreases from plant and animal respiration.

The full model is a pair of coupled equations:

$$x_{t+1} = \underbrace{a_t \cdot \sin(2\pi f t)}_{A(t)} - \underbrace{\left\{m + a_t\left[\frac{w_{t-1}}{K_w + w_{t-1}}\right]\right\}}_{f(w,x,t)} + \underbrace{D_t(x_t)}_{g(x,t)} \qquad \text{(Equation S2)}$$

$$a_{t+1} = a_t \times \left\{\frac{a'_{max} - a'_{min}}{1 + \exp(-s \cdot n_t - d)} + a'_{min}\right\}$$

We discuss each of A, $f(\bullet)$, and $g(\bullet)$ in turn; individual terms are summarized in Table S1.

Table S1 – Interpretation and units of terms in the model of oxygen dynamics within pitcher-plant fluid (Equation S2).

Term	Meaning	Units
a_t	maximum amount of oxygen infused at mid-day (amplitude of sine wave for diurnal release of O_2)	mg/L initialized at $a_0 = 10$
a'_{min}, a'_{max}	minimum or maximum possible augmentation of photosynthesis as a result of nutrient uptake from organic-matter decomposition	mg/L set at $a'_{min} = 0$, $a'_{max} = 2$
d	inflection point of the sigmoidal curve relating additional nutrients to augmentation of photosynthesis by organic-matter decomposition	mg set at $d = 0.5$
D_t	Recovery of oxygen as a function of available oxygen (diffusion) and photosynthesis (augmented by bacterial activity), offset by respiration	mg/L
f	constant adjusting sine wave of diurnal release of O_2 for frequency of measurements	1/t set at $f = 1/1440$
K_w	half-saturation constant for prey consumption	mg/min one of $K_w = 0.1$, 0.01, or 0.001
m	amount of oxygen used for basal metabolism of bacteria	mg/L $m = 1$
n_t	quantity of nutrients released from organic-matter decomposition; it is a function of w_t and x_t.	mg/L
s	steepness of the sigmoidal curve relating additional nutrients to augmentation of photosynthesis by organic-matter decomposition	dimensionless
t	time (frequency of model iterations)	minutes
w_t	mass of prey at time t	mg
x_t	concentration of oxygen in the pitcher fluid	mg/L

1.2 Details of the model

A – The proximal environmental factor $A(t)$, which determines baseline oxygen concentration, is diurnal photosynthesis: pitcher-plant leaves take up CO_2 from the water and release O_2 back into it (4, 5). We approximate diurnal release of O_2 (in mg/L) as a zero-truncated sine wave (Figure S1), with a daily peak at mid-day and no O_2 release at night:

$$A(t) = a \cdot \sin(2\pi f t) \qquad \text{(Equation S2.1)}$$

where a is amplitude (equal to the maximum amount of oxygen infused at midday). The constant f within the sine function adjusts for frequency of measurements (iterations in the model), which we make every minute (t is in units of minutes). Hence, $f = 1/1440$ (the reciprocal of number of minutes per day). Without loss of generality, we initialize $a = 10$ (see below, Equation S2.5), start our time series at sunrise ($t = 1$), set day-length at 12 hours, and truncate $A(t) = 0$ at night, *i.e.*, for $t \in \{720, 1440\}$.

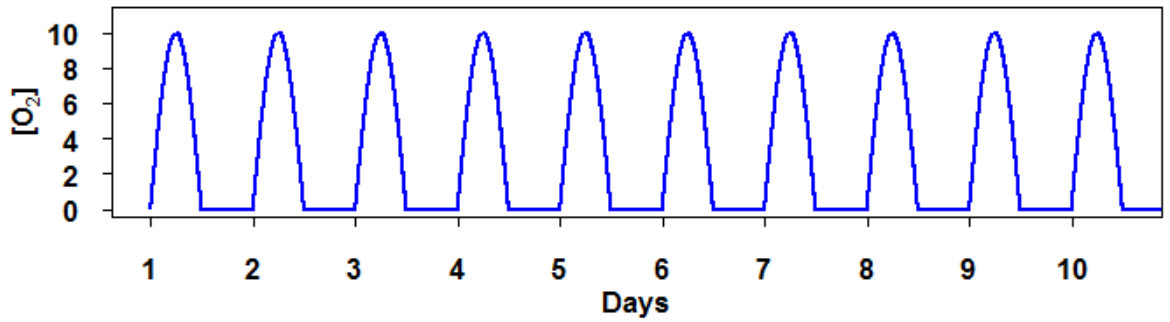

Figure S1 – Simulated infusion of O_2 into a pitcher-plant leaf due to diurnal photosynthesis (A) in Equation S2.1.

$f(w,x)$ – Oxygen is lost from the system rapidly as prey is consumed by bacteria; this respiration is equivalent to biological oxygen demand (BOD). Because both aerobic and anaerobic bacteria will digest organic matter with more-or-less equal efficiency (6), we assume sufficient, equilibrial numbers of bacteria to process prey at a fixed, negative exponential rate:

$$w(t+1) = ae^{-b[w(t)]} \qquad \text{(Equation S2.2)}$$

This model is sensible because easily digested parts of prey, such as fat bodies, are processed first, whereas difficult to digest parts, such as chitin, break down more slowly and are processed later (7); field observations suggest that a single 75-µg wasp can be completely consumed over a 48-hour period in a pitcher with 5 ml of liquid. Thus, in our initial model runs, we set a = 20 mg and b = 4 (mg mg^{-1} d^{-1}) (Figure S2).

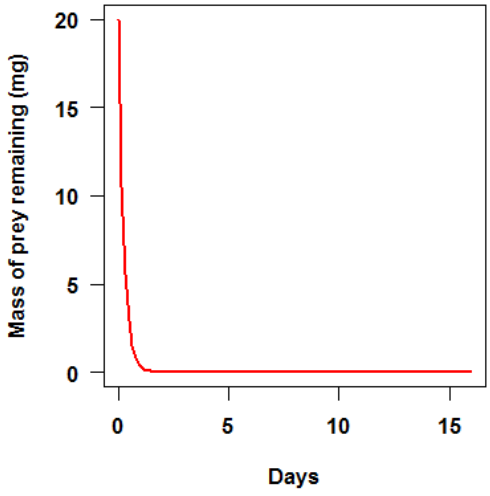

Figure S2 – Simulated decomposition of prey, assuming a single wasp can be consumed in 48 hours in a 5-ml pitcher, from Equation S2.2.

We model oxygen lost from the system due to prey consumption (= 1 – BOD) to be a saturating (Holling Type-II) function of prey remaining, which itself is a function of the maximum amount of oxygen infused at midday (a from Equation S2.1, iteratively augmented by a' as detailed below using Equations S2.4 and S2.5); the mass of prey remaining (w); a half-saturation constant for prey consumption (K_w), which determines how much prey is leftover each day and would be carried over to the next day; and the amount of oxygen used for basal metabolism of bacteria (m):

$$O_2 \text{ lost}(t) = f(w,x,t) = m + a\left[\frac{w(t-1)}{K_w + w(t-1)}\right] \qquad \text{(Equation S2.3)}$$

In our initial model runs, we set m = 1 and K_w = 0.1, 0.01, or 0.001 (Figure S3).

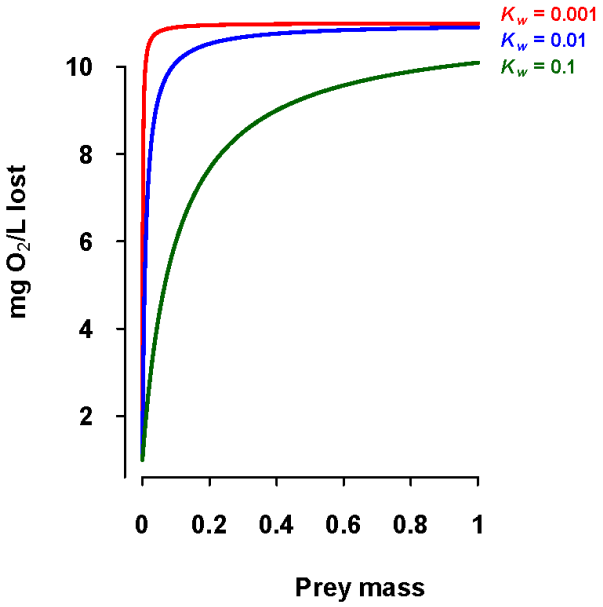

Figure S3 – Simulated loss of oxygen from biological oxygen demand as a function of available oxygen (*a*) and prey mass available (*w*), for three different values of K_w from Equation S2.3.

$g(x)$ – Oxygen is replenished in the system in three ways. First, there is some diffusion from the atmosphere into the pitcher fluid. Second, there is oxygen production through daily photosynthesis (2). Because diffusion only happens at the surface of the pitcher fluid, and the "mouth" area of the pitcher is nearly 10× smaller than the surface area of the pitcher itself (8), the amount of oxygen replenished by diffusion is likely to be much less than that provided by photosynthesis; in our model runs, we considered only replenishment from photosynthesis (Equation S2.1).

Most importantly, there is a positive feedback loop described by the a_{t+1} term in Equation S2 that relates prey mineralization to the uptake of mineralized nutrients by the plant, and the use of these nutrients to increase photosynthetic rate (9). Dead insect prey (ground wasps in our experiment) is a mixture of carbon and mineral nutrients (the C:N ratio is ≈ 6:1). As prey are broken down and mineralized, nutrients are slowly released by the bacteria and in turn, these nutrients (especially ammonia) are taken up readily by the plant (5). Numerous observations and experiments have demonstrated that carnivorous plants are nutrient (primarily nitrogen) limited (10), and that photosynthetic rates of pitcher plants are enhanced following prey additions (10). We model these processes with a pair of equations.

First, the amount of nutrients released, *n*, is a function of prey mass (*w*) and available oxygen (*x*) used by bacteria to break down and mineralize the prey (Figure S4):

$$n(t) = \frac{w(t)x(t)}{c} \qquad \text{(Equation S2.4)}$$

where *c* is a scaling constant (we set *c* = 100).

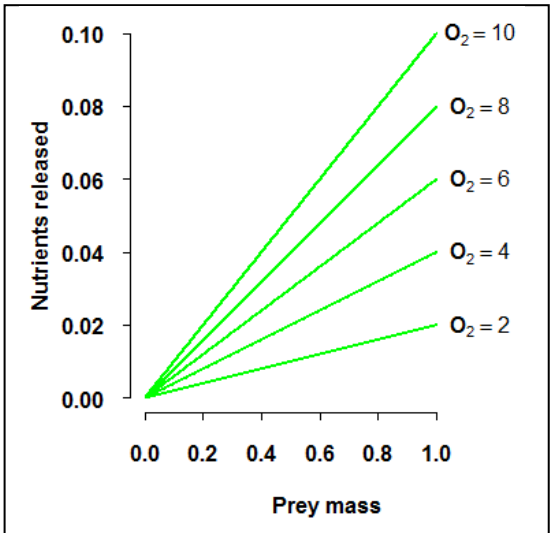

Figure S4 – Nutrients released as a function of prey mass (*w*) and *available* oxygen (*x*), from Equation S2.4.

Because nutrients taken up by the plant could be used to make additional enzymes involved in photosynthesis (8), we model uptake as a sigmoidal, saturating relationship between additional nutrients and an augmentation of the peak rate of photosynthesis (a) in Equation S2.1 (Figure S5).

$$a'(t) = \frac{a'_{max} - a'_{min}}{1 + \exp -[s * n(t) - d]} + a'_{min} \qquad \text{(Equation S2.5a)}$$

$$a(t+1) = a(t) \times a'(t) \qquad \text{(Equation S2.5b)}$$

In Equation S2.5a, a'_{min} is the minimum possible augmentation of photosynthesis, which we initially set = 0; a'_{max} is the maximum possible augmentation, which we initially set = 2, s is the steepness of the increase (= 10), and d is the inflection point of the curve (= 0.5). Augmentation evolves as leftover prey (*i.e.*, prey not completely broken down on one day) accumulates (within the $n(t)$ term) and is further mineralized.

Equation S2.5b iteratively updates the maximum possible photosynthetic rate (a in Equation S2.1). Because this mineralization and conversion is assumed to be a slow process, the update occurs only once each day, as shown in Figure S6.

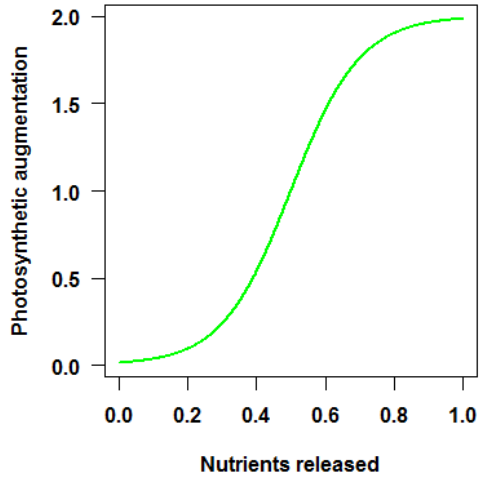

Figure S5 – Modeled (Equation S2.5a) effects of nutrients released by decomposition of prey on augmentation factor (*a´*) by which maximum photosynthetic rate *a* (in Equation S2.1) would be increased.

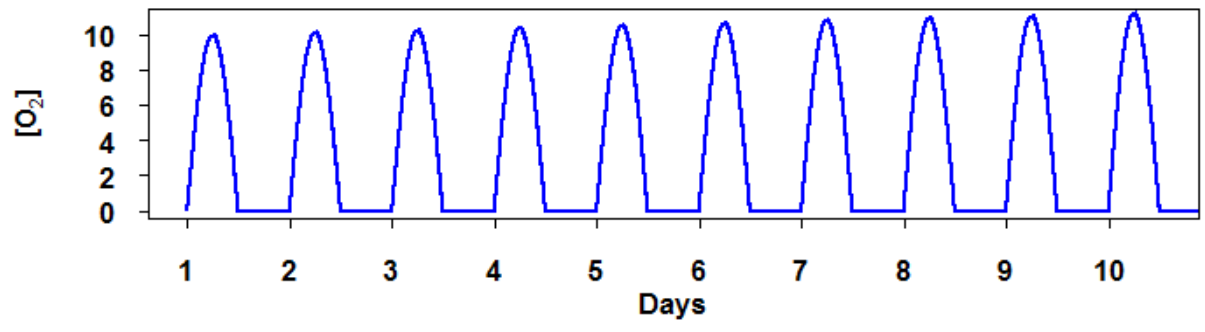

Figure S6 – Simulated infusion of oxygen into a pitcher plant leaf with photosynthetic rate increased daily following mineralization of prey (using Equations S2.4 – S2.5b).

1.3 Model behavior

Model behavior for three levels of organic-matter loading – none, low, and high – and three levels of half-saturation constants K_w (from Equation S2.3; see Figure S3) are shown in Figures S7-S9. Model runs began at sunrise (0600 hrs) and prey was added at noon (red triangles in Figure S7). Five days of runs are shown using different colors for each day. Because we modeled both PAR and oxygen evolution (photo-synthesis) using a sine wave, there is a gradual and continuous increase or decrease in $[O_2]$ with diurnal PAR in the control (no prey addition). This differs from the behavior of real plants, in which photosynthesis would follow a Michelis-Menten-type function with rapid saturation (and which could be modeled as a square wave). We also neglect stochasticity in the system. Regardless of whether photosynthesis is modeled as a sine wave or a square wave, when prey is added, two alternative states (alternate attractors) are visible, with a strong tipping point following

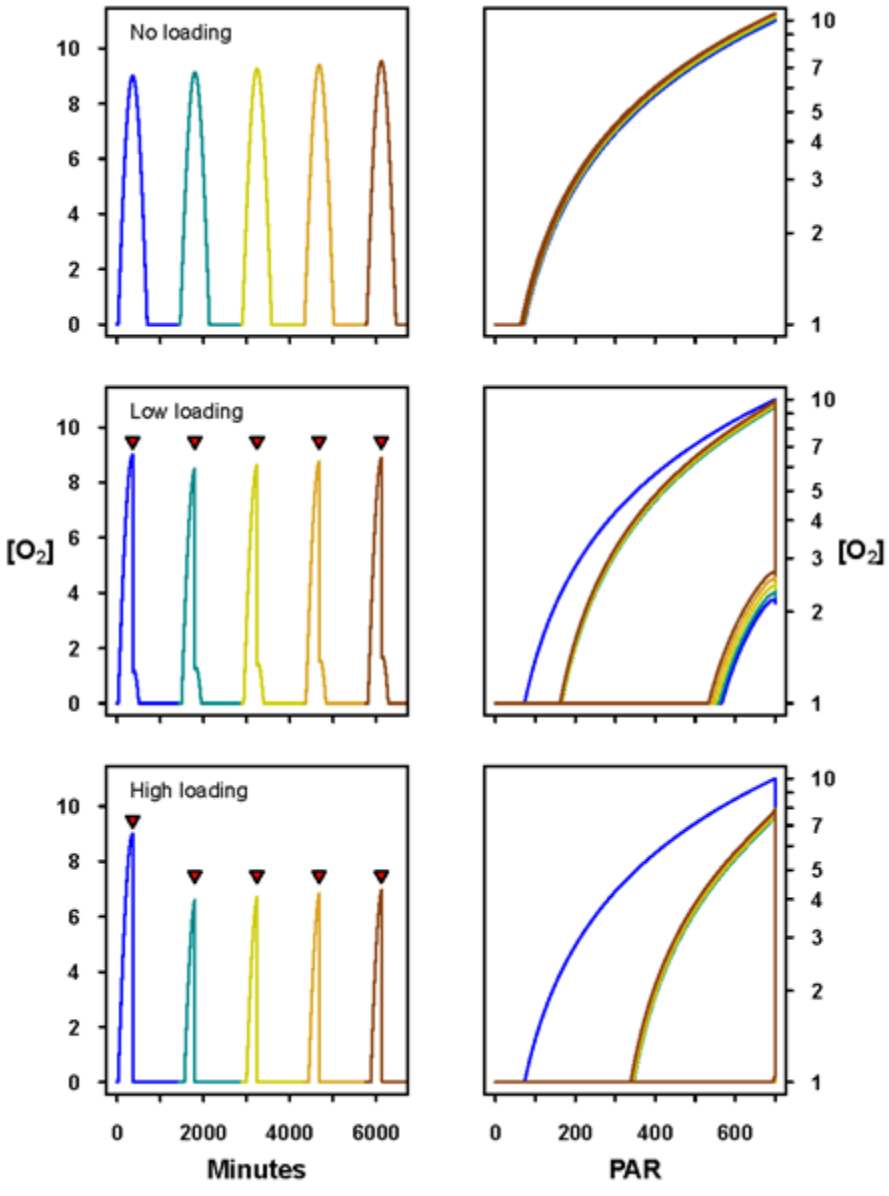

Figure S7 – Dynamics of the pitcher-plant model (Equations S1 – S2.5), for three levels of prey loading (none, low, high prey additions) with prey half-saturation constant K_w (Equation S3) = 0.1.The left column shows the diurnal oxygen concentration for the three prey-additions, with timing of prey addition indicated by inverted red triangles. The rapid drop in $[O_2]$ following prey addition is caused by high BOD, but the recovery is equally rapid because of the high value of K_w. Each 24-hour segment in the time series is illustrated with a different color (day 1 = blue, day 5 = brown)**.**The right column shows the corresponding relationship between $[O_2]$ and PAR for each time series.

prey addition. The magnitude of the half-saturation constant controls in large part the difference between the control (aerobic) state and the alternative (anaerobic) state, because it determines how much organic matter is not broken down and is carried over to the next day for additional decomposition. A large half-saturation constant (Figure S7) results in prey being broken down rapidly and the system recovering relatively quickly. As the half-saturation constant decreases, immediate oxygen loss (BOD) increases (Figure S3), and the system collapses rapidly into an anaerobic state (Figure S9).

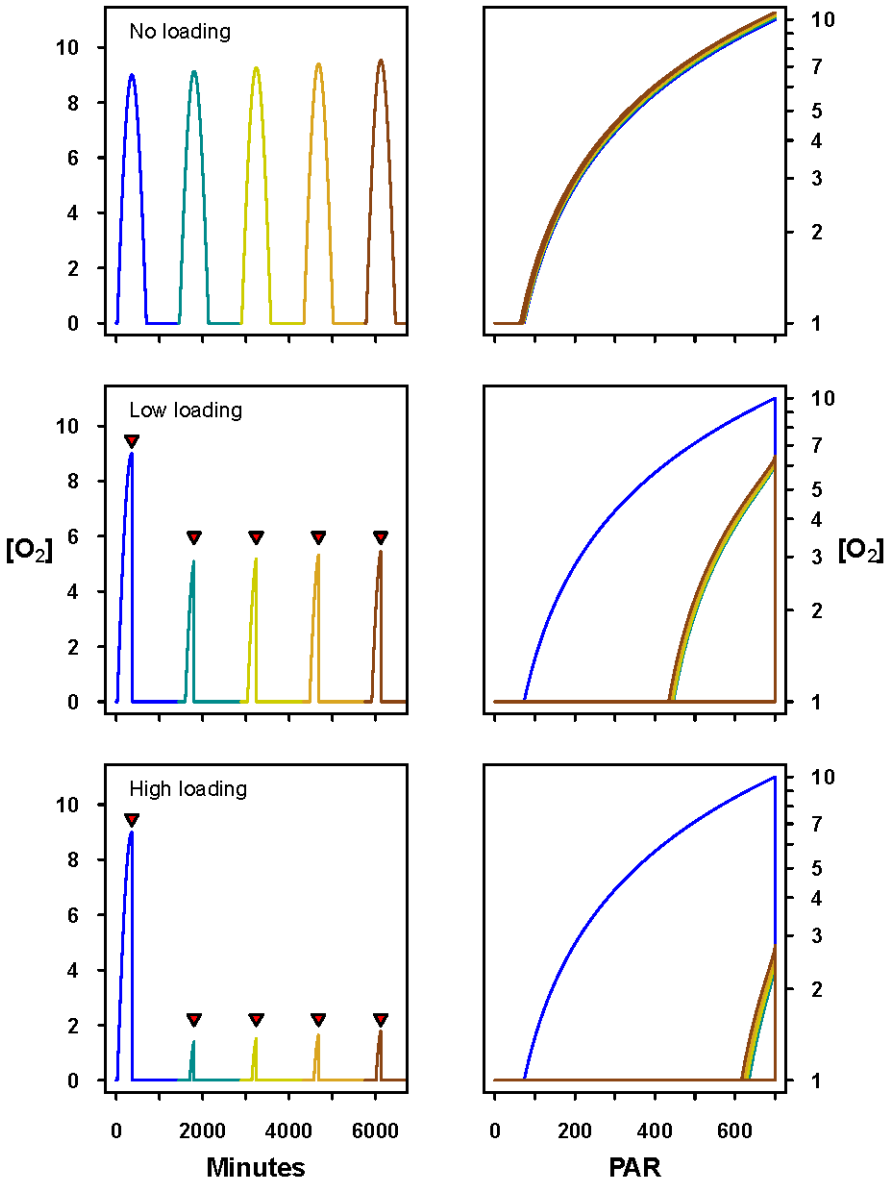

Figure S8 – Dynamics of the pitcher-plant model (Equations S1 – S2.5), for three levels of prey loading (none, low, high prey additions) with prey half-saturation constant K_w (Equation S3) = 0.01.The left column shows the diurnal oxygen concentration for the three prey-additions, with timing of prey addition indicated by inverted red triangles. The rapid drop following prey addition is caused by high BOD, but the recovery is slowed because of the lower value of K_w. Each 24-hour segment in the time series is illustrated with a different color (day 1 = blue, day 5 = brown). The right column shows the corresponding relationship between $[O_2]$ and PAR for each time series.

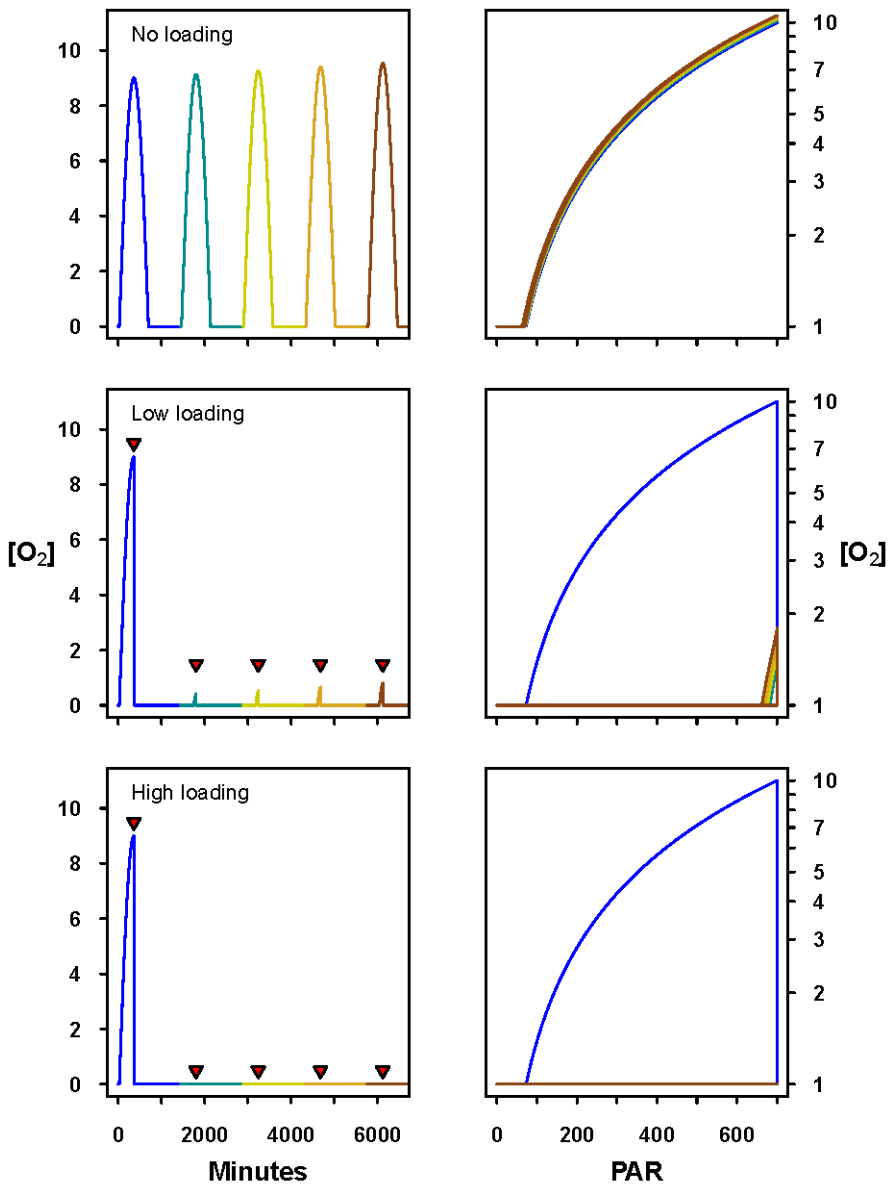

Figure S9 – Dynamics of the pitcher-plant model (Equations S1 – S2.5), for three levels of prey loading (none, low, high prey additions) with prey half-saturation constant K_w (Equation S3) = 0.001.The left column shows the diurnal oxygen concentration for the three prey-additions, with timing of prey addition indicated by inverted red triangles. The rapid drop following prey addition is caused by high BOD, but the recovery is even slower than in Fig S8 rapid because of the very low value of K_w.. Each 24-hour segment in the time series is illustrated with a different color (day 1 = blue, day 5 = brown). The right column shows the corresponding relationship between $[O_2]$ and PAR for each time series. As in Figure S8, there is a clear second attractor in this example. In the high organic-matter loading simulation (bottom), the second attractor is a tight point at the lower right corner of the plot, not even a small cycle (as in the low organic-matter loading simulation).

1.3 Programming and availability of code

The model was coded in Mathematica v8.0. Model code is available from the Harvard Forest Data Archive, dataset HF-205 (http://harvardforest.fas.harvard.edu/data-archive).

2. Additional statistical analyses

2.1 Analysis of frequency distribution of daytime oxygen concentration

The combined frequency distribution of a system can illustrate how it is affected by environmental drivers. If the underlying environmental driver is unimodal, then multiple modes of the frequency distribution suggest locations of the basins of attraction of alternative states of the system (11-12).

In our experimental system, baseline [O_2] is controlled by the plant's photosynthesis, and the primary environmental driver is photosynthetically active radiation (PAR) (Equation S2.1 and Figure S2.1, above). Daytime PAR during our experiment was unimodal (Figure S10), but Fig. 1 and Fig. S13 (next section) in the main text illustrate that the "normal" relationship between diurnal PAR and diurnal [O_2] breaks down as prey (organic matter) is added to the aquatic *Sarracenia* microecosystem.

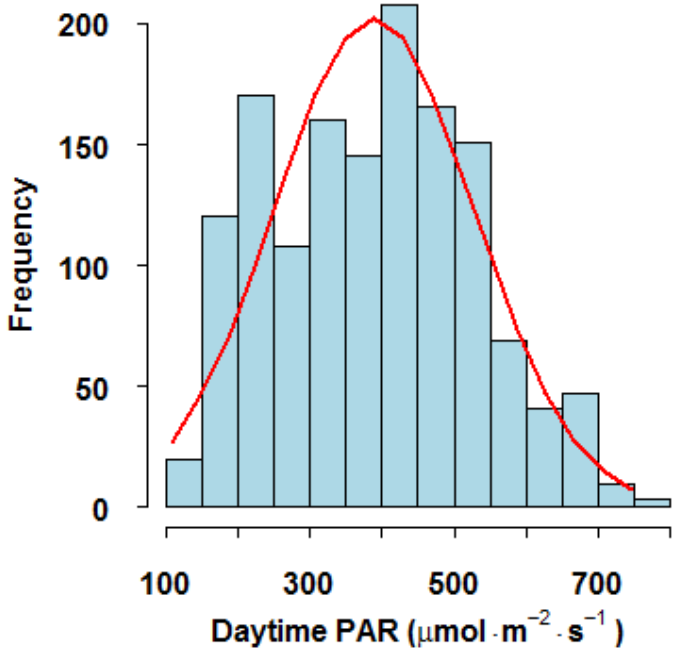

Figure S10 – Frequency distribution of daytime photosynthetically active radiation (PAR) during the prey-addition experiments.

The number of modes in the combined frequency distribution of [O_2] of the different treatments was identified with normal mixture modeling and model-based clustering using the mclust package in R, version 3.4 (13). With 7090 total observations, the Bayesian Information Criterion (BIC) identified 4-9 modes as equally plausible (Figure S11); BIC declined rapidly with fewer modes (Figure S11). Thus, parsimony suggests that the overall distribution would be best fit with a four-modal distribution (Figures S12; Table S2).

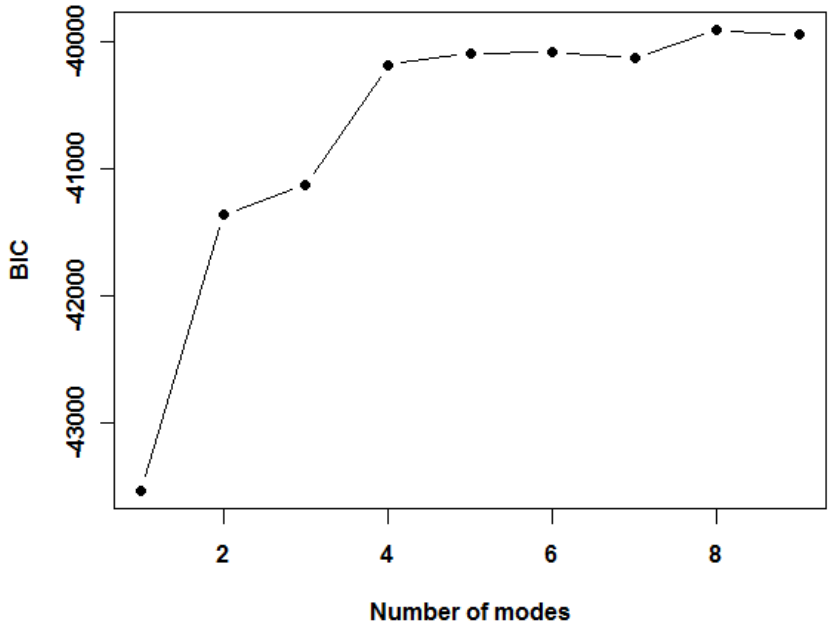

Figure S11 – BIC of the number of modes in the joint frequency distribution of $[O_2]$.

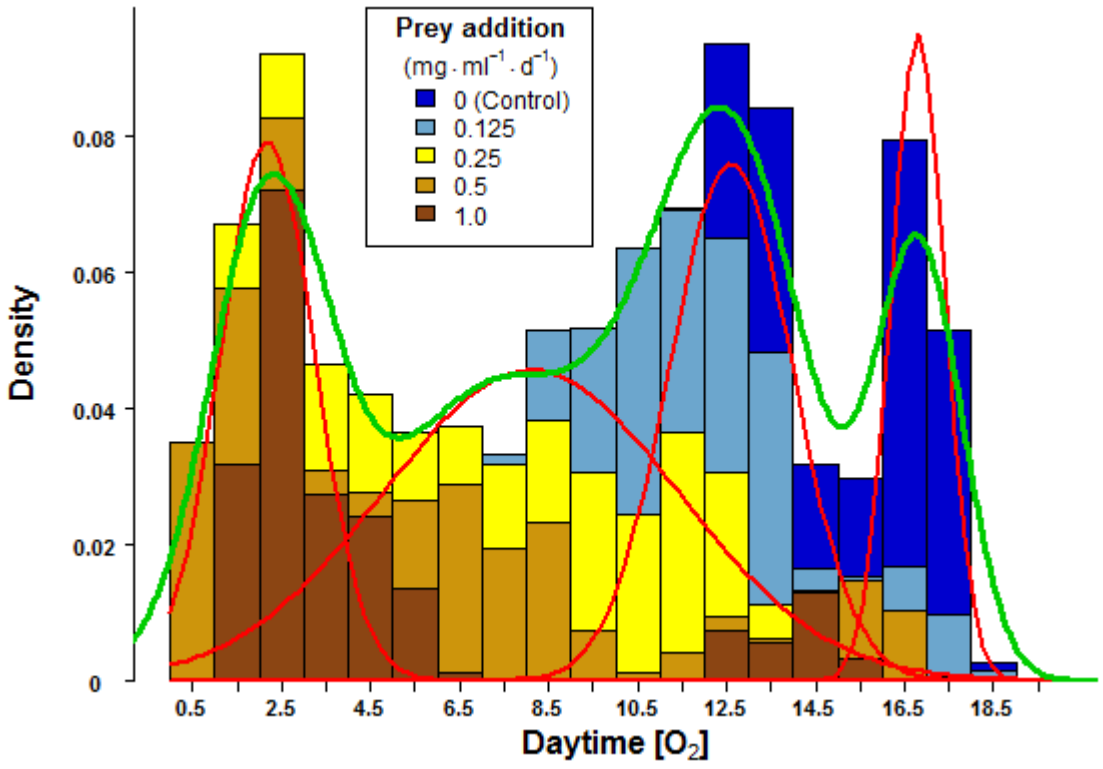

Figure S12 – Probability density functions (red) for each of the modes identified in the joint distribution of $[O_2]$ in the prey-addition experiments. The best-fit (based on BIC) overall probability density function (green) has four modes.

Table S2 – Best-fit combinations of normal distributions fitted to the frequency distribution of [O_2] in the prey-addition experiment (Fig. S12).

Mode	μ	σ	proportion
1	1.682	1.070	0.21
2	7.554	3.322	0.38
3	12.146	1.378	0.26
4	16.272	0.605	0.15

2.2 Supplemental analysis of time-series data

The time-series analysis presented in Figure 1 of the main text presents means and confidence intervals of raw data (main text Figures 1A-1E) and then time-series analysis of residuals following detrending relative to the controls. Although detrending relative to the controls does allow for comparisons among the effects of different prey-addition treatments, observed increases in temporal variance following such detrending are not evidence for critical slowing down (*csd*). Rather, evidence for *csd* should be sought by analysis of individual time series or of replicate time series within a given treatment. Here we illustrate the raw data, followed by analysis of individual time series detrended and decycled relative to themselves.

The raw time series and the mean for each prey-addition treatment and the diurnal cycle in photosynthetically available radiation (PAR: μmol m^{-2} s^{-1}) are shown in Figure S13. As suggested by Figures 1A-1E in the main text, the differences among replicates are generally small (except for one replicate within the highest prey-addition treatment), and variance among treatments exceeds variance within treatments (main text Table 1). The diurnal re-oxygenation of the pitcher-plant fluid predominantly associated with photosynthesis (and PAR; bottom time series in Figure S13) is clear in the controls, but falls apart to different degrees in the four prey-addition treatments. This is seen more clearly in the plots of [O_2] as a function of PAR (Figure S14; these plots of raw [O_2] show qualitatively similar, albeit more exaggerated, patterns as seen in Figures 1K-1O of the main text, in which we plotted the residuals (relative to controls) of [O_2] as a function of PAR).

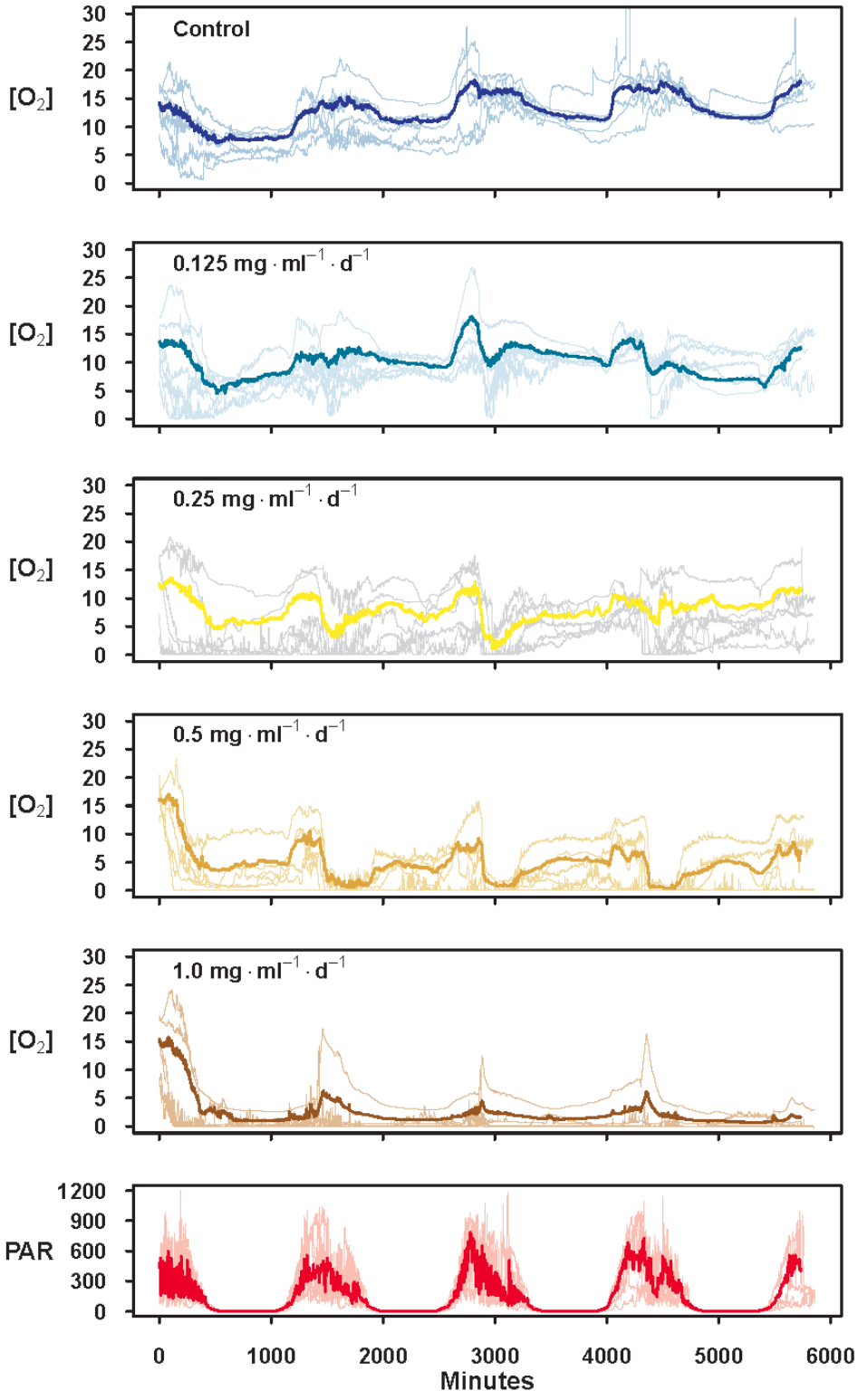

Figure S13 – Untransformed time series of [O_2] in pitcher-plant microecosystems in response to five experimental prey-addition treatments (top five panels) and PAR (lowest panel). In each panels, the light lines are the six individual replicates, and the dark line is the mean response to treatment.

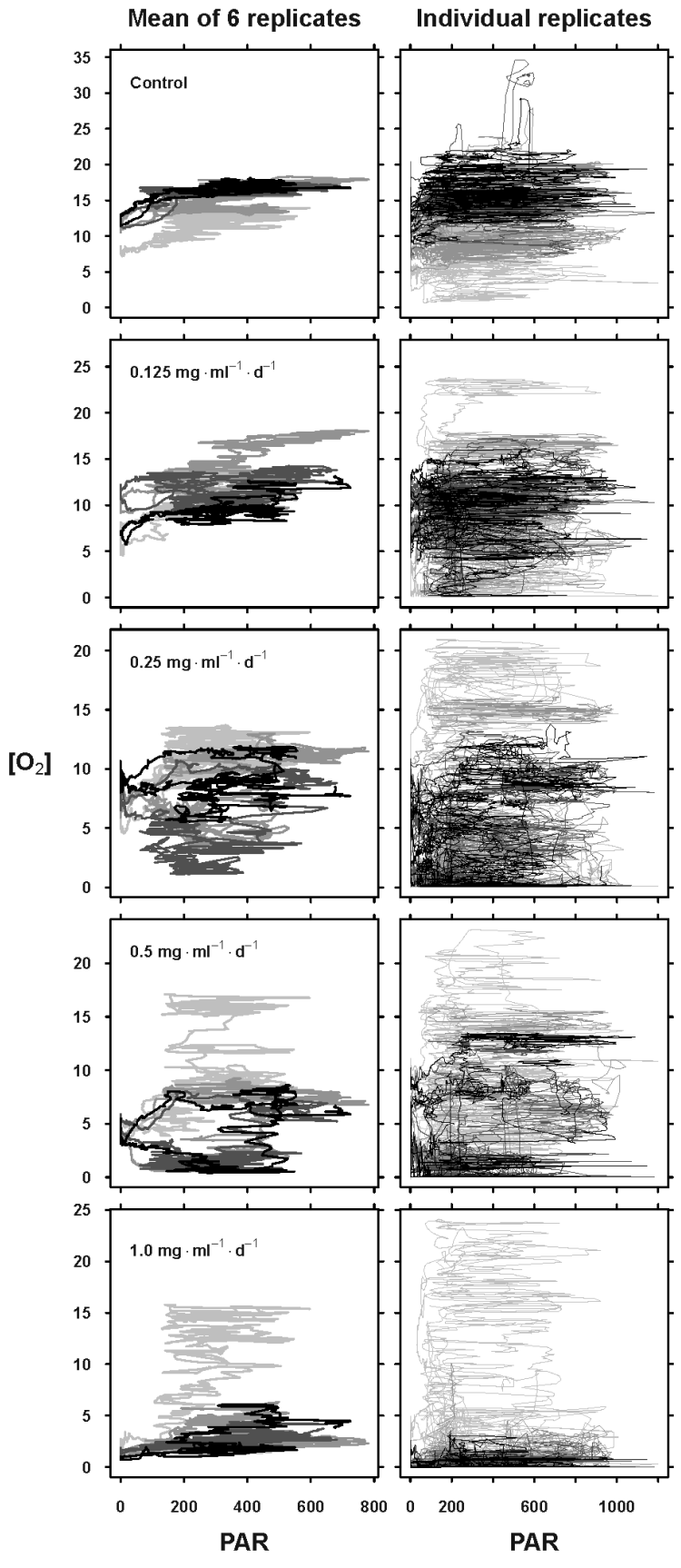

Figure S14 – Plots of [O_2] as a function of PAR for each prey-addition treatment (top to bottom: controls to 1.0 mg ml^{-1} d^{-1}. Gray-scale indicates the four days of prey additions, from day 1 (light gray) through day 4 (black). Plots in the left column are the means of all six replicates in each treatment, whereas plots in the right column shows time-series traces of all six individual replicates.

Each individual time-series from a given replicate was detrended and decycled using local regression (*loess* in R), with the span set = 0.125. We chose this moving window (12.5% of the data) because it corresponds to approximately 12 hours and appropriately smooths a daytime (or night-time) cycle. The individual traces and the averages for each treatment are shown in Figure S15. As expected, all such detrended and decycled time series have mean ≈ 0, and periodicity was eliminated from all of the time series because of the chosen span for the local regression.

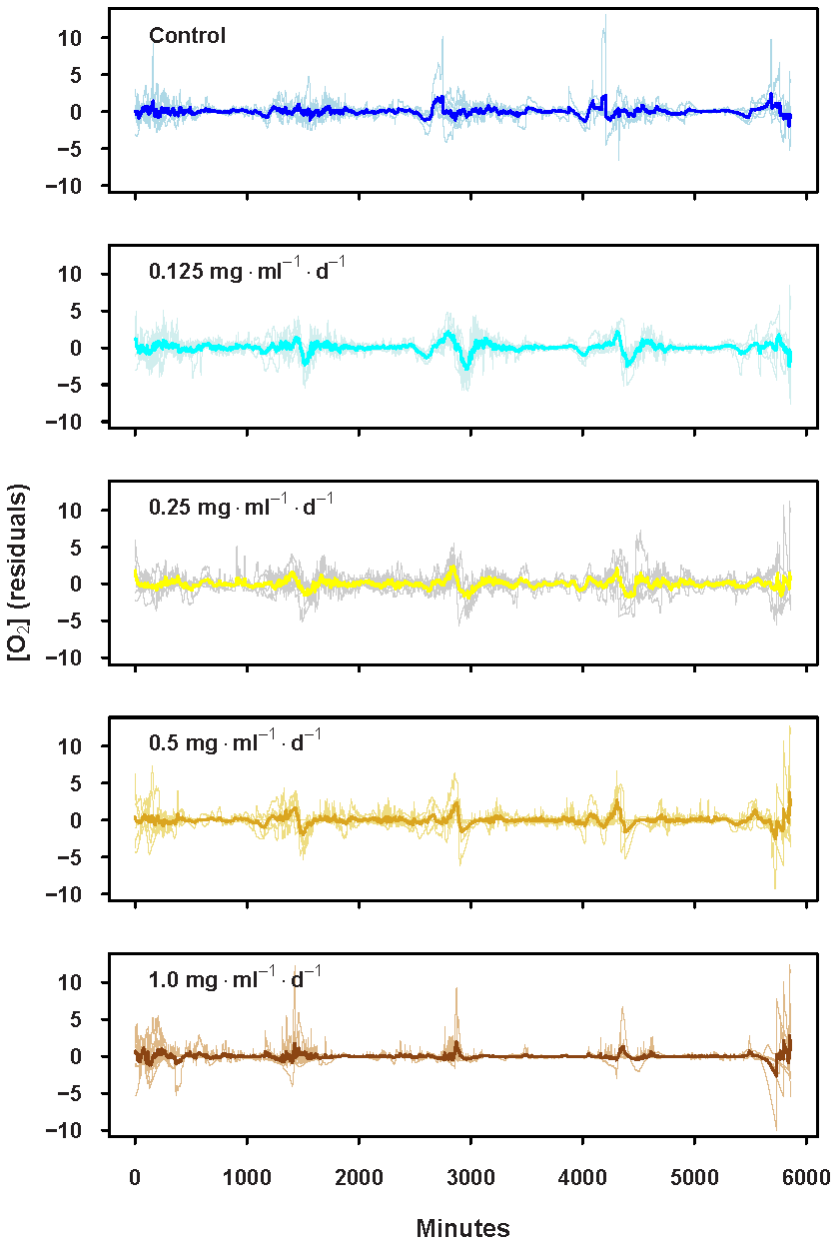

Figure S15 – Time-series of residuals of [O_2] in pitcher-plant microecosystems in response to five experimental prey-addition treatments. Residuals for each replicate time-series were calculated as the difference between the raw data and a local regression (loess) on the data. In each panel, the light lines are the six individual replicates, and the dark line is the mean response to treatment.

Last, we examined changes in the temporal variance of the detrended and decycled time series (Figure S16) as a potential indicator of *csd* (11).

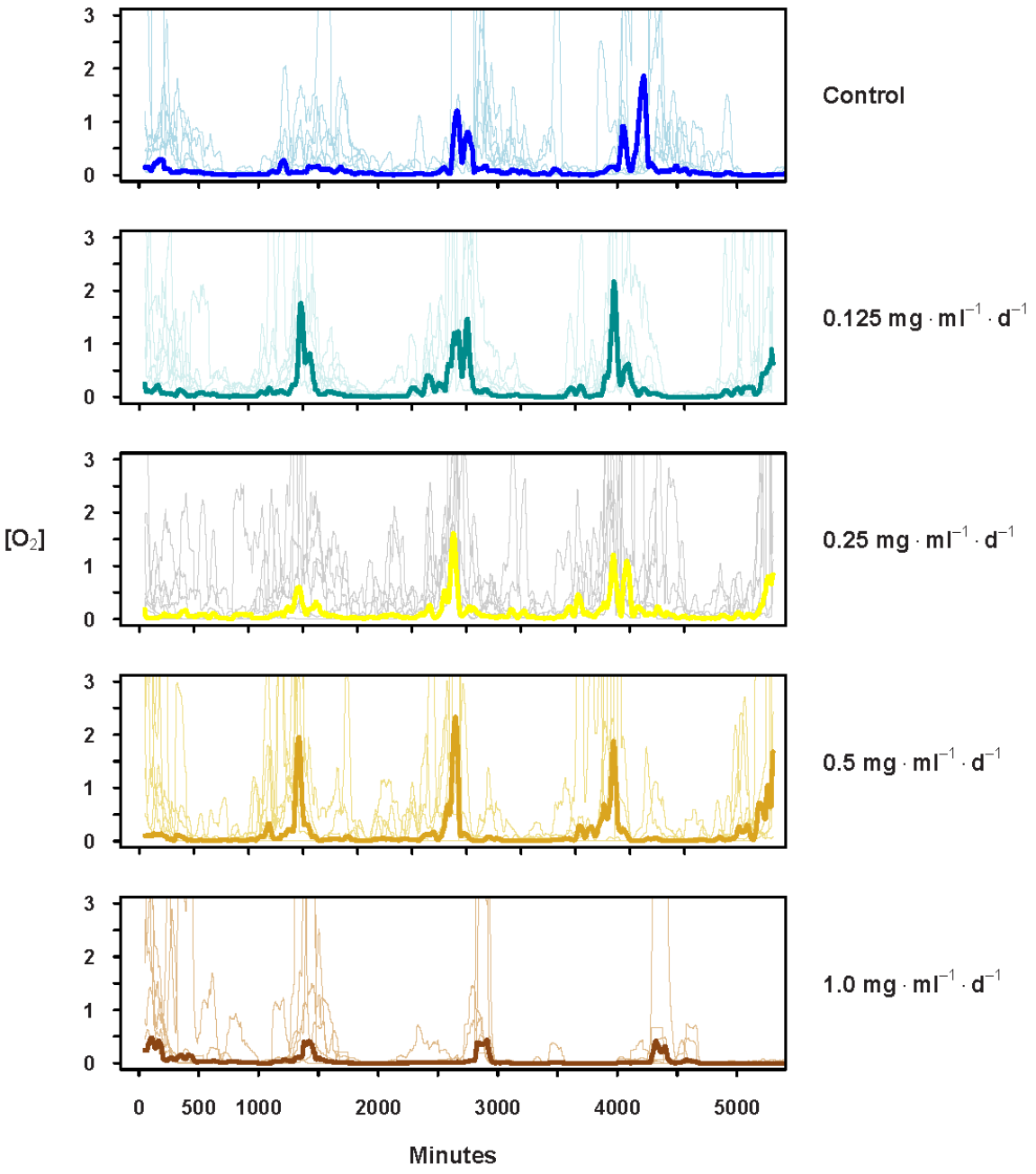

Figure S16 – Temporal variance (rolling window, size = 100 minutes) of the six individual time series (light lines) and of the average time series (dark lines) of [O_2] in each of the five prey-addition treatments, detrended and decycled as illustrated in Figure S15.

Although Figure S16 illustrates daily noise in [O_2] associated with biological oxygen demand following daily prey addition (Equation S2.3 and Figure S3), that quickly dissipates in the control treatment (no prey addition). The three intermediate prey additions show more variance across the time series, as well as a pronounced uptick in variance towards the end of the experiment. In contrast, the highest prey addition treatment (bottom panel of Figure S16) shows little change in variance after the first day. In this treatment, variance is highest on the first day, suggesting that the treatment tipped the system into a new regime after either the first feeding (0 minutes in Figure S16) or the second feeding (1441 minutes in Figure S16).

References

1. Odum HT (1956) Primary production in flowing water. Limnol Oceanogr 1(2):102-117.
2. Bradshaw WE, Creelman RA (1984) Mutualism between the carnivorous purple pitcher plant and its inhabitants. Am Mid Nat 112(2):294-303.
3. Scheffer M, Carpenter S, Foley JA, Folke C, Walker B (2001) Catastrophic shifts in ecosystems. Nature 413(6856):591-596.
4. Cameron CJ, Donald GL, Patterson CG (1977) Oxygen-fauna relationships in the pitcher plant, *Sarracenia purpurea* L. with special reference to the chironomid *Metriocnemus knabi* Coq. Can J Zool 55(12):2018-2023.
5. Bradshaw WE, Creelman RA (1984) Mutualism between the carnivorous purple pitcher plant and its inhabitats. Am Midl Natur 112(2):294-304.
6. Murphy MG, Condon S (1984) Comparison of aerobic and anaerobic growth of *Lactobacillus plantarum* in a glucose medium. Arch Microbiol 138(1):49-53.
7. Baiser B., Ardeshiri R, Ellison AM (2011) Species richness and trophic diversity increase decomposition in a co-evolved food web. PLoS One 6: e20672.
8. Ellison AM, Gotelli NJ (2002) Nitrogen availability alters the expression of carnivory in the northern pitcher plant *Sarracenia purpurea*. *Proc Nat Acad Sci USA* 99(7):4409-4412
9. Farnsworth EJ, Ellison AM (2008) Prey availability directly affects physiology, growth, nutrient allocation, and scaling relationships among leaf traits in ten carnivorous plant species. J Ecol 96(1): 213-221.
10. Ellison AM (2006) Nutrient limitation and stoichiometry of carnivorous plants. Plant Biol 8(6): 740-747.
11. Scheefer M, Carpenter SR, Lenton, TM, Bascompte J, Brock W, Dakos V, van de Koppel J, van de Leemput, IA, Levin, SA, van Nes, EH, Pascual M, Vandermeer J (2012) Anticipating critical transitions. Science 338(6105): 344-348.
12. Scheffer M, Hirota M, Holmgren M, Van Nes EH, Chapin FS III (2012) Thresholds for boreal biome transitions. *Proc Nat Acad Sci USA* 109(52): 21384-21389.
13. Fraley C, Raftery AE (2012) MCLUST version 3 for R: normal mixture modeling and model-based clustering. Department of Statistics, University of Washington, Technical Report 504. http://www.stat.washington.edu/research/reports/2012/tr504.pdf.